#### **Research Article**

Shuo Li, Sohail Ahmad\*, Kashif Ali, Ahmed M. Hassan, Waleed Hamali, and Wasim Jamshed

### A mathematical approach for modeling the blood flow containing nanoparticles by employing the Buongiorno's model

https://doi.org/10.1515/ntrev-2023-0139 received May 23, 2023; accepted September 25, 2023

Abstract: A mathematical model has been suggested for the numerical study of blood flow in a vessel due to the pumping action of the heart. Blood is assumed to contain some impurities in the form of chemically reactive species (undergoing a first-order irreversible reaction) and, being a hybrid nanofluid, also contains the nano-sized solid particles, thus forming a homogeneous mixture which is subjected to a pressure gradient (of trigonometric nature) in the horizontal direction. Human vessel is subjected to a transverse magnetic field and is presumed to be filled with plaque which is considered as a porous medium, and is mathematically modeled by applying the Darcy-Forchheimer theory. The nonlinear nature of the governing equations steered toward the decision of using the numerical approach to obtain the solution of the governing system, which led to the discovery of a linear concentration variation across the vessel at higher values of the Reynolds number. Finally, a 38% rise in the heat transfer has been noted due to the presence of solid particles in the human blood.

**Keywords:** hybrid nanofluid, blood flow, Darcy–Forchheimer medium, pressure gradient, fully implicit scheme

**Kashif Ali:** Department of Basic Sciences and Humanities, Muhammad Nawaz Sharif University of Engineering and Technology, Multan 60000, Pakistan

**Ahmed M. Hassan:** Faculty of engineering, Future University in Egypt, New Cairo, Egypt

**Waleed Hamali:** Department of Mathematics, College of Science, Jazan University, 45142, Jazan, Saudi Arabia

**Wasim Jamshed:** Department of Mathematics, Capital University of Science and Technology (CUST), Islamabad, 44000, Pakistan

#### **Nomenclature**

magnetic field strength (kg $s^{-1}$ $A^{-1}$ )
molecular diffusivity (m <sup>2</sup> s <sup>-1</sup> )
acceleration due to gravity (m s <sup>-2</sup> )
rate of chemical reaction (s <sup>-1</sup> )
thermal conductivity (W m <sup>-1</sup> k <sup>-1</sup> )
permeability (m²)
dimensionless Prandtl number
dimensionless Reynolds number
velocities (m s <sup>-1</sup> )
kinematic viscosity (m <sup>2</sup> s <sup>-1</sup> )
electrical conductivity (S m <sup>-1</sup> )
density (kg m <sup>-3</sup> )
volume fraction of Cu (mol m <sup>-3</sup> )
stream function (m <sup>2</sup> s <sup>-1</sup> )
thermal diffusivity (m <sup>2</sup> s <sup>-1</sup> )
volume fraction of Fe <sub>3</sub> O <sub>4</sub> (mol m <sup>-3</sup> )

#### 1 Introduction

The pulsatile flow involves periodic variations and, due to this fact, it has several important uses in the fields of science and biomechanics. A periodic pressure fluctuation is essential for the integrity of the tissues which cause the smooth blood flow. It is comprehensive to interpret the pulsatile flow, so that, the prominent benefits in the biomechanics as well as blood flow may be characterized. Thomas et al. [1] assessed perforator veins by means of arterial pulsations in the lower limbs of heat-stressed and healthy humans. The superficial veins were connected with perforator veins that drained into the deep veins. They noted pulsatility in ten different persons which was normal for blood flow. Ryu et al. [2] used a flexible strain sensor in order to measure the circumferential strain generated by a pulsating fluid flow. This sensor comprised of a Triton-X treatment with polydimethylsiloxane that enhanced the adhesive property of carbon nanotubes nanoparticles.

<sup>\*</sup> Corresponding author: Sohail Ahmad, Department of Basic Sciences and Humanities, Muhammad Nawaz Sharif University of Engineering and Technology, Multan 60000, Pakistan, e-mail: sohailkhan1058@gmail.com Shuo Li: School of Mathematics and Data Sciences, Changji University, Changji, Xinjiang 831100, China

It was noticed from experiment that pulsating fluids' flow rate could be accurately measured by the flexible strain sensor. Versatile applications of the several fluid flows, that are beneficial in the modern technology, can be studied from the literature [3–7].

An axisymmetric non-Newtonian pulsatile flow was simulated by Cheffar et al. [8]. They found the numerical solutions by employing the finite difference technique. They investigated the wall shear stress distribution, external acceleration, pressure gradient and structural properties. A mathematical model was established by Praljak et al. [9] to explore the interaction of fluid with elastic kidney tubule provided that pressure was pulsatile. In this study, an idea to prevent the chronic kidney diseases using dynamic pathology is presented. Mittal et al. [10] studied the pulsatile flow using large-eddy simulation and direct numerical simulation. The flow was taken in a one-sided constricted channel. The results revealed that the Reynolds number caused an increase in the characteristic shear-layer frequency. Painter et al. [11] established relations between energy dissipation, shear force and pulsatile blood flow using Murray's law. According to this law, moving blood encompasses shear force which is constant on the inner vessel walls. However, they derived the results for constant blood flow.

Recently, bio-magnetic fluids have been extensively studied due to their bioengineering and biomedical applications. Examples of bio-magnetic fluids involve: magnetic hyperthermia and medical devices (blood pumps and magnetic tracers), reduction in bleeding during surgeries, magnetic wound treatment, cell separation and targeted drug delivery. The blood comprises of intercellular protein, hemoglobin compound and cell membrane; therefore, it is a prominent example of biomagnetic fluid. An application of magnetohydrodynamic (MHD) effect on blood flow is to reduce the blood flow friction which not only controls the blood pressure but also controls the cholesterol level. A numerical investigation on the MHD pulsatile flow was conducted by Amos and Ogulu [12]. They noticed that the fluid speed decreased with an enhancement in the magnetic field. This phenomenon might increase the work load on heart and give rise to heart attack. However, they suggested to increase flow pressure to circumvent this problem. MHD pulsatile flow in a different shaped channel was scrutinized by Bandyopadhyay and Layek [13]. It was claimed that the axial velocity would flatten with an increase in magnetic field parameter. Eldesoky [14] examined the impact of periodic body acceleration on MHD pulsatile flow by changing the relaxation time. Blood was considered to act as an electrically conducting and incompressible fluid. Their results designated that the relaxation time had a substantial effect on axial velocity and shear

stress. Abbas *et al.* [15] and Ali *et al.* [16] presented numerical analysis of pulsatile flow under MHD environment using explicit finite difference scheme and explicit Runge–Kutta method, respectively.

The distinct types of nanoparticles have their own thermal characteristics which possess enhanced thermal features. A non-Newtonian flow of nanoparticles, on the horizontal surface, was elaborated by Zeeshan et al. [17] taking the impact of catalytic chemical reaction. Ahmad et al. [18] developed an algorithm to determine the numerical solution of hybrid nanofluids containing graphene oxide and iron oxide particles together with engine oil as base fluid. They used order reduction method to simulate the governing problem. An axisymmetric flow involving the homogeneous/heterogeneous reactions over a cylinder was studied by Pattnaik [19]. The cylinder contained the Darcy-Forchheimer porous medium through which the fluid was flowing. Different types of fluid flows such as Carreau fluid flow, Maxwell fluid and Sutterby nanofluid were investigated by Salahuddin et al. [20-22]. Karmakar et al. [23] scrutinized the hybrid nano-blood flow with trihybrid nanoparticles.

An artificial suspension of hybrid nanoparticles in the pulsatile flow can provide assistance to magnetize and stabilize the flow. An electrically conducting blood flow together with nanoparticles can also act as ferromagnetic fluid and, as a consequence, velocity of fluid increases gradually. An utmost attention by the research community has been given to investigate the pulsatile flow comprising of hybrid nanoparticles. The blood-based hydromagnetic pulsatile flow through porous channel involving couple stress hybrid nanofluid was investigated by Rajamani and Reddy [24]. The hybrid nanoparticles copper oxide (CuO) and gold (Au) were suspended in the blood which was the base fluid. The perturbation technique was used to convert the partial differential equations into ordinary differential equations and then shooting method together with RK fourth-order approach was adopted to determine the numerical solution of the problem. The MHD pulsatile flow of hybrid nanoparticles (gold and alumina) was probed by Govindarajulu and Reddy [25]. The blood was assumed to be a third-grade base fluid. An increase in non-Newtonian parameter and Hartmann number caused a reduction in the velocity. Selimefendigil [26] examined water hybrid nanofluid pulsatile flow subject to oscillating rectangular double slot jets whereas Manchi and Ponalagusamy [27] analyzed the pulsatile hybrid nanofluid flow (Ag-TiO<sub>2</sub>/blood) subject to uniform magnetic field. Pulsatile flow of non-Newtonian Casson fluid in a channel having symmetric walls was considered by Bukhari et al. [28]. The vorticity-stream function form was obtained from governing model equations which

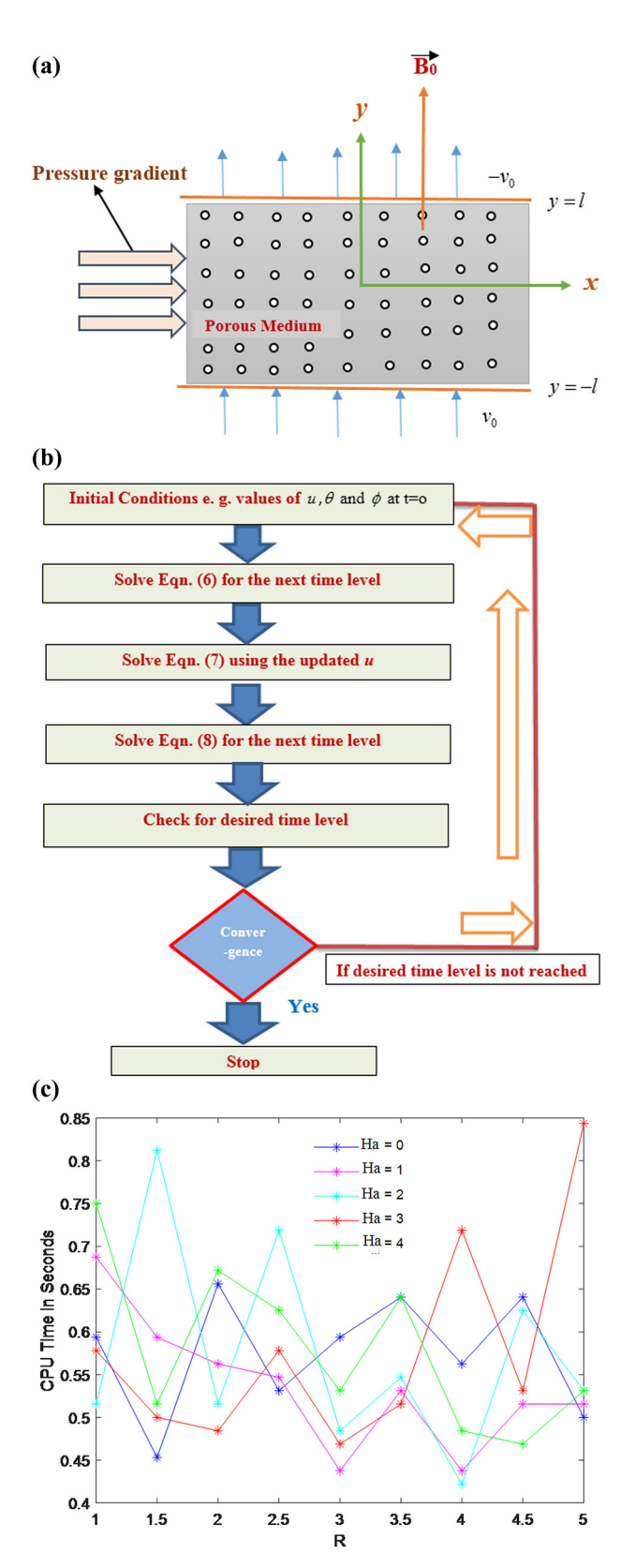


**Figure 1:** (a) Schematic diagram of the problem. (b) The flowchart diagram of the explicit RK method. (c) Change in the CPU time with the magnetic parameter.

was then solved numerically. Further aspects of the pulsatile flow can be studied from previous studies [29–34].

To the authors' best knowledge, no research was found dealing with the modeling of the blood as a hybrid nanofluid under an oscillating pressure gradient. Therefore, a comprehensive analysis of nanofluid flow comprising hybrid nanoparticles under the MHD environment is presented in this study. The blood flow dynamics is interpreted in either case of pure or hybrid nanofluids with the change in emerging parameters. Another objective, in the present work, is to justify how much a Darcy-Forchheimer flow is affected by the applied pressure gradient having oscillatory and static components. The available literature evidently discloses that no study is reported yet to interpret the pulsatile natured nanofluid flow with rheological properties, specifically, under the magnetic field environment. The current learning will, expectantly, fill the gap in this direction. Numerical treatment to the highly coupled and nonlinear equations is carried out via a fully implicit numerical scheme. The potential of the current study can be found in pharmacological engineering (drug delivery systems) and various biomedical systems.

# 2 Description of mathematical model

An electrically conducting fluid flow is assumed to be occurring inside a parallel plate channel through a porous medium. The applied pressure gradient with oscillatory and static components causes the motion of fluid. The lower channel plate encompasses the injection phenomenon whereas the suction takes place at the upper one. A suitable Cartesian coordinate system is specified on channel plates which are located at  $y = \pm l$  (Figure 1a). Fluid is flowing between parallel plates of a channel with wall transpiration. The flow is two dimensional as well as incompressible and laminar. Furthermore, the nature of flow is pulsatile. The model equations also involve Joule heating and viscous dissipation.

The general form of the governing equations can be composed as follows:

Now, we discuss the governing model equations under the prescribed conditions.

#### 2.1 Momentum equation

The momentum equation, in the light of Nakamura and Sawada model [35], has the following form:

$$\frac{\partial u}{\partial \tau} + v_0 \frac{\partial u}{\partial y} = -\frac{1}{\rho_{\text{hnf}}} \frac{\partial p}{\partial x} + v_{\text{hnf}} \frac{\partial^2 u}{\partial y^2} - \sigma_{\text{hnf}} \frac{B_0^2 u}{\rho_{\text{hnf}}} - \frac{v_{\text{hnf}}}{k_{\text{P}}} u$$

$$-bu^2. \tag{2}$$

The above equation is interlinked with the Navier–Stokes momentum equation and the Forchheimer law. The last two terms are illustrated by the Forchheimer law. The blood is assumed to be the nanofluid, in the concerned problem, which contains two different types of solid particles.

The terms involved in equation (2) are expressed as follows:

 $\rho_{\rm hnf}$  denotes the density of the hybrid nanofluid,

b shows the inertial drag coefficient,

p represents the pressure,

 $\tau$  signifies the dimensional time,

 $k_{\rm P}$  demonstrates the permeability of the porous medium,

u symbolizes the horizontal velocity component,

 $B_0$  defines the magnetic field strength,

 $v_0$  designates the wall transpiration velocity,

 $\nu_{hnf}$  describes the kinematic viscosity of the hybrid nanofluid, and

 $\sigma_{hnf}$  expresses the electrical conductivity of the hybrid nanofluid.

#### 2.2 Energy equation

The governing energy equation of the problem has the following form:

$$\frac{\partial T}{\partial \tau} + v_0 \frac{\partial T}{\partial y} = \alpha_{\rm hnf} \frac{\partial^2 T}{\partial y^2} + \frac{\mu_{\rm hnf}}{(\rho c_{\rm p})_{\rm hnf}} \left( \frac{\partial u}{\partial y} \right)^2 + \frac{\sigma_{\rm hnf} B_0^2}{(\rho c_{\rm p})_{\rm hnf}} u^2, \quad (3)$$

where temperature of the fluid is represented by the symbol T and  $\alpha_{\rm hnf}$  is the thermal diffusivity of the hybrid nanofluid. The term  $\frac{\partial^2 T}{\partial y^2}$  in equation (3) is used for the thermal diffusion whereas the first derivative terms of the same equation represent the thermal convection phenomenon. The involvement of diffusion is due to the temperature difference at both channel walls which occurs because walls are placed at different temperatures. It is assumed initially that wall transpiration effects (suction/injection) are negligible at plates or walls due to which a linear change in the temperature is noticed across the channel. Afterward, the suction/injection effects are imposed and temperature is noticed to be varying non-linearly (see temperature profiles in Section 4).

#### 2.3 Concentration equation

The chemically reactive species are also contained in the blood inside the channel. Obviously, the flow involves the mass transfer due to the presence of species. The concentration is denoted by C having unit  $\text{mol/m}^3$  and involves the homogeneous mixture. Because of the species involvement, the flow possesses first order irreversible and homogeneous reaction taking place within the fluid. The fixed concentrations  $C_1$  and  $C_2$  are taken, respectively, at the lower and upper walls. The mass transfer equation with concentration differences at both walls is given by

$$\frac{\partial C}{\partial \tau} + v_0 \frac{\partial C}{\partial y} = D^* \frac{\partial^2 C}{\partial y^2} - k(C - C_{\rm m}), \tag{4}$$

where k is the rate constant of chemical reaction that describes how fast the chemical reaction occurs within the channel and D expresses the mass diffusivity. The negative sign with the last term of equation (4) designates the fact that the species are being destroyed by the chemical reaction.

Finally,  $C_{\rm m} = \frac{C_1 + C_2}{2}$  is taken as the reference concentration (used in the mathematical modeling) also known as characteristic concentration.

#### 2.4 Boundary conditions

The proposed boundary conditions in the present case (for t > 0) are as follows:

$$u = 0, C = C_1, T = T_1 \text{ at } y = -l$$
  
 $u = 0, C = C_2, T = T_2 \text{ at } y = l,$  (5)

where  $C_1$ ,  $T_1$ ,  $C_2$  and  $T_2$  are the constant concentrations and temperatures at the lower as well as upper channel wall, respectively.

## 2.5 Non-dimensional coordinates and equations

The non-dimensional coordinates are introduced as follows:

$$U = \frac{u}{v_0}, \, \xi = \frac{x}{a}, \, \eta = \frac{y}{a}, \, t = \frac{v_0}{a} \tau, \, P = \frac{p}{\rho_{\rm f} v_0^2},$$

$$\theta = \frac{T - T_{\rm m}}{T_2 - T_{\rm m}}, \, \phi = \frac{C - C_{\rm m}}{C_2 - C_{\rm m}},$$
(6)

which convert the governing equations in the following form:

$$\frac{\partial U}{\partial t} + \frac{\partial U}{\partial \eta} = -\frac{\partial P}{\partial \xi} + \frac{1}{\text{Re}} \Delta_0 \frac{\partial^2 U}{\partial \eta^2} - \text{Ha} \cdot d_3 (1/d_{01}) U - \frac{1}{\lambda} (\Delta_0) U - F_{\text{r}} U^2,$$
(7)

$$\frac{\partial \theta}{\partial t} + \frac{\partial \theta}{\partial \eta} = \frac{1}{RPr} \cdot (d_4/d_5) \frac{\partial^2 \theta}{\partial \eta^2} + \frac{Ec}{R} \cdot (1 - \psi_1)^{-2.5}$$

$$\times (1 - \psi_2)^{-2.5} (1/d_5) \left(\frac{\partial u}{\partial \eta}\right)^2$$

$$+ EcHa \cdot (d_3/d_5) u^2,$$
(8)

$$\frac{\partial \phi}{\partial t} + \frac{\partial \phi}{\partial n} = \frac{1}{\text{Sc}} \frac{\partial^2 \phi}{\partial n^2} - \frac{\gamma}{R} \phi, \tag{9}$$

where

$$\Delta_0 = \frac{(1 - \psi_1)^{-2.5} \times (1 - \psi_2)^{-2.5}}{(1 - \psi_2) \left[1 - \psi_1 + \psi_1 \frac{\rho_{s_1}}{\rho_f}\right] + \psi_2 \frac{\rho_{s_2}}{\rho_f}},\tag{10}$$

$$d_{01} = (1 - \psi_2) \left[ 1 - \psi_1 + \psi_1 \frac{\rho_{s_1}}{\rho_f} \right] + \psi_2 \frac{\rho_{s_2}}{\rho_f}, \tag{11}$$

$$d_{3} = \frac{\sigma s_{2} + 2\sigma_{\rm bf} - 2\psi_{2}(\sigma_{\rm bf} - \sigma s_{2})}{\sigma s_{2} + 2\sigma_{\rm bf} - 2\psi_{2}(\sigma_{\rm bf} - \sigma s_{2})} \times \frac{\sigma s_{1} + 2\sigma_{f} - 2\psi_{1}(\sigma_{f} - \sigma s_{1})}{\sigma s_{1} + 2\sigma_{f} + 2\psi_{4}(\sigma_{f} - \sigma s_{1})},$$
(12)

$$d_{4} = \frac{k_{s_{2}} + 2k_{bf} - 2\psi_{2}(k_{bf} - k_{s_{2}})}{k_{s_{2}} + 2k_{bf} + 2\psi_{2}(k_{bf} - k_{s_{2}})} \times \frac{k_{s_{1}} + 2k_{f} - 2\psi_{1}(k_{f} - k_{s_{1}})}{k_{s_{2}} + 2k_{f} + 2\psi_{1}(k_{f} - k_{s_{2}})},$$
(13)

$$d_5 = (1 - \psi_2) \left[ 1 - \psi_1 + \psi_1 \cdot \frac{\rho_{s_1}}{c p_{s_1}} \frac{\rho_f}{c p_f} \right] + \psi_2 \cdot \frac{\rho_{s_1}}{c p_{s_1}} \frac{\rho_f}{c p_f}.$$
 (14)

The nanoparticles volume fraction of copper is  $\psi_1$  and that of iron oxide is  $\psi_2$ . The thermo-physical properties of both nanoparticles as well as base fluid are provided in Table 1.

#### 2.6 Parameters of the problem

The governing non-dimensional parameters of the problem are as follows:

$$\lambda = \frac{k_p v_0}{a v_f}$$
 is the Darcy parameter,

Re = 
$$\frac{av_0}{v_f}$$
 is the Reynolds number,

 $F_{\rm r}$  = ab is the Forchheimer quadratic drag parameter,

Table 1: Thermophysical attributes of nanoparticles and blood

Properties	Cu(s <sub>1</sub> )	Blood (f)	Fe <sub>3</sub> O <sub>4</sub> (s <sub>2</sub> )
σ (S m <sup>-1</sup> )	5.96 × 10 <sup>7</sup>	0.8	25,000
k (W m <sup>-1</sup> K <sup>-1</sup> )	401	3,594	6
$\rho$ (kg m <sup>-3</sup> )	8,933	1,063	5,200
$C_{\rm p} \ ({\rm J \ kg^{-1} \ K^{-1}})$	385	0.492	670

Sc =  $\frac{av_0}{D}$  is the Schmidt number,

Ha =  $\frac{\sigma_f B_0 a}{\rho_f v_0}$  is the magnetic parameter,

 $Pr = \frac{v_f}{a_s}$  is the Prandtl number,

 $\gamma = \frac{ka^2}{v_{\rm f}}$  is the chemical reaction parameter,

Ec =  $\frac{v_0^2}{c_0 \Delta T}$  is the Eckert number.

The pressure gradient  $\frac{\partial P}{\partial \xi}$  in terms of its frequency  $\omega$  can be stated as follows:

$$-\frac{\partial P}{\partial \xi} = P_{\rm S} + P_0(\cos \omega t),\tag{15}$$

where the static and the oscillatory components of the pressure gradient are, respectively, represented by  $P_0$  and  $P_0$ .

The boundary constraints now take the form

$$\eta = -1: U = 0, \theta = \varphi = -1,$$

$$\eta = 1: u = 0, \theta = \varphi = 1 \quad \forall t > 0.$$
(16)

At the beginning, when the fluid is at rest, the concentration and temperature vary linearly with  $\eta$  (across the channel); however, the initial conditions at this stage take the form

$$U = 0, \theta = \varphi = \eta \ \forall -1 \le \eta 0 \le 1 \text{ at } t = 0.$$
 (17)

### 3 Numerical solution and methodology

The appearance of systems (6)–(8) is complex natured which involves highly nonlinear and coupled equations. Nevertheless, the analytic solution of such system is almost impossible. If so, it might be so much time consuming. Therefore, we follow a completely implicit numerical approach which is based on the forward difference approximation for the time derivative, and central differences for spatial derivatives appearing in the governing equations. The discretized form of the governing Eqs. (6)–(8) may thus be written as follows:

6 — Shuo Li et al. DE GRUYTER

$$\frac{u_{i}^{n+1} - u_{i}^{n}}{dt} + \frac{u_{i+1}^{n+1} - u_{i-1}^{n+1}}{2h}$$

$$= -\left(\frac{\partial p}{\partial \xi}\right)^{n+1} \frac{\Delta_{0}}{Re} \left(\frac{u_{i+1}^{n+1} - 2u_{i}^{n+1} + u_{i-1}^{n+1}}{h^{2}}\right)$$

$$- Ha \cdot d_{3} \left(\frac{1}{d_{0}1}\right) u_{i}^{n+1} - \frac{\Delta_{0}}{\lambda} u_{i}^{n+1} - F_{r} \cdot u_{i}^{(n+1)^{2}},$$

$$\frac{\theta_{i}^{n+1} - \theta_{i}^{n}}{dt} + \frac{\theta_{i+1}^{n+1} - \theta_{i-1}^{n+1}}{2h}$$

$$= \frac{1}{Re \cdot Pr} \left(\frac{dn}{df}\right) \left(\frac{\theta_{i+1}^{n+1} - 2\theta_{i}^{n+1} + \theta_{i-1}^{n+1}}{h^{2}}\right),$$

$$\frac{\phi_{i}^{n+1} - \phi_{i}^{n}}{dt} + \frac{\phi_{i+1}^{n+1} - \phi_{i-1}^{n+1}}{2h} = \frac{1}{Sc} \left(\frac{\phi_{i+1}^{n+1} - 2\phi_{i}^{n+1} + \phi_{i-1}^{n+1}}{h^{2}}\right)$$

$$- \frac{\gamma}{Re} \phi_{i}^{n+1}.$$
(18)

The numerical scheme configuration is described in Figure 1b.

**Table 2:** Comparison of velocity  $u(\eta)$  variation across the channel for a certain limiting case

η	<i>u</i> (η)	
	Ashraf et al. [36]	Present
-0.8	0.447484	0.447595
-0.4	1.014633	1.014744
0	1.212160	1.212271
0.4	1.065582	1.065693
0.8	0.496384	0.496495

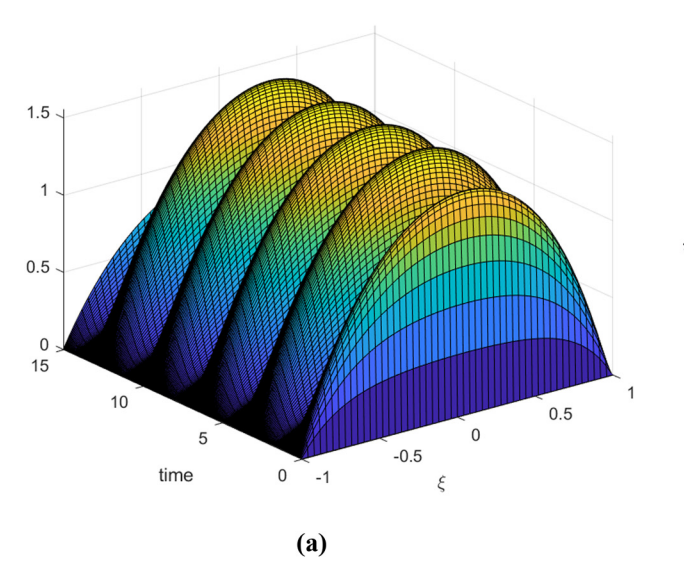
The code is validated by means of a numerical data comparison (Table 2) which not only appraises the code efficiency but also makes us confident to develop the result effectually. Figure 1c depicts the change in CPU time against different values of the magnetic parameter.

#### 4 Results and discussion

With blood as a base fluid containing two different types of nanoparticles, this section is devoted to the primary understanding of the way the relevant parameters tend to influence the momentum, thermal and concentration profiles for the present problem when a periodic force drives the flow in a horizontal channel. With the physical domain being shown in Figure 1a, following values of the governing parameters have been considered throughout the present investigation:

 $\lambda$  = 0.5,  $F_{\rm r}$  = 0.75, Re = 1, Pr = 21, Sc = 2,  $\gamma$  = 0.5,  $p_0$  = 5,  $p_{\rm s}$  = 7,  $\omega$  = 2, Ha = 0.5,  $\psi_1$  = 0.05 and  $\psi_2$  = 0.05, unless otherwise mentioned.

The numerical outcomes are monitored (for velocity, temperature and concentration) subject to distinct spatial step sizes, at a certain time level. Variation in the velocity profile with time, across the channel, is given in Figure 2a. We notice a sort of repetitive behavior or cycles in the flow field, with  $\omega$  being the parameter determining the frequency of such cycles. It is easy to note that, compared to the forthcoming cycles, the maximum flow velocity during the first cycle is relatively lower, as the fluid was initially



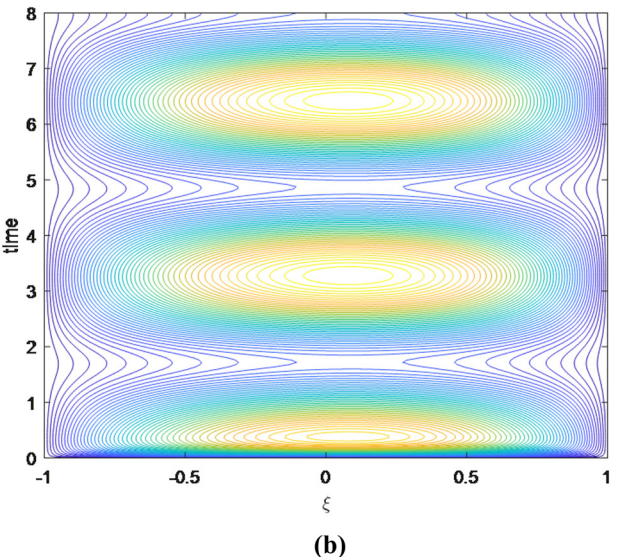


Figure 2: (a) Variation in the velocity field, with time and (b) contours of velocity field across the channel.

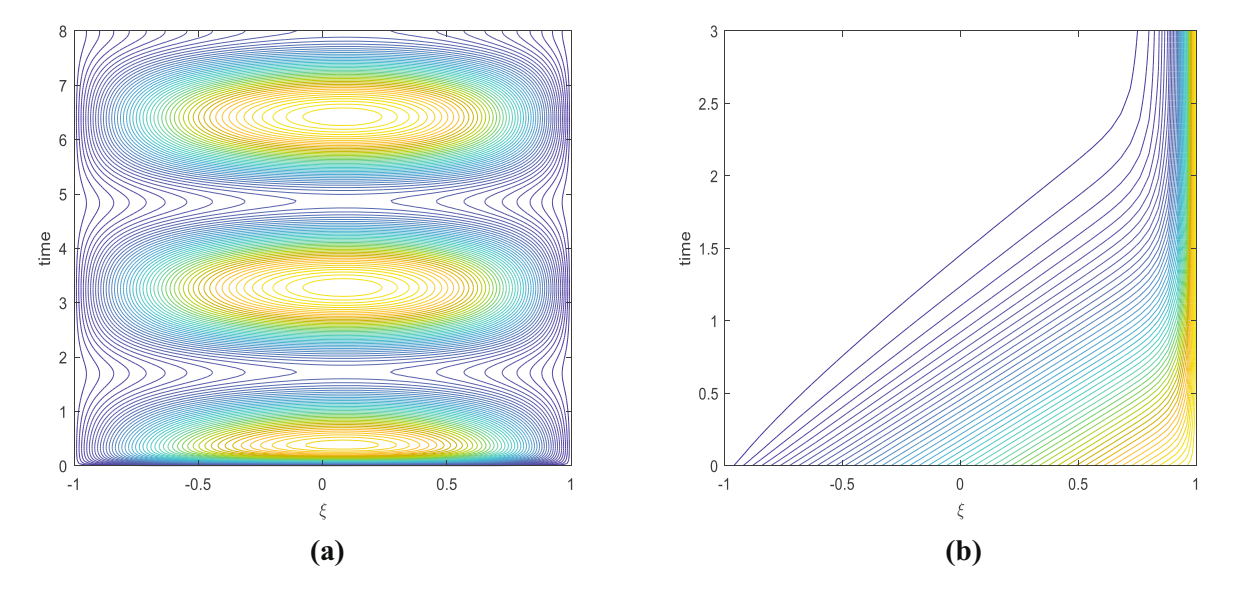


Figure 3: (a) Variation in the temperature field, with time and (b) isotherms across the channel.

stagnant and the applied force due to the pressure gradient was relatively less effective compared to the case when the flow acquires certain momentum after some time. This is the reason why the initial cycle is not symmetric compared to the forthcoming ones. Contours of velocity field across the channel can be examined from Figure 2b.

Initially the two channel walls have stagnant fluid in between, and consequently two different (fixed) wall temperatures lead to a linear temperature variation. However, as the driving force comes into play, we notice a flattening effect on the thermal distribution in a major part of the channel which means that most of the fluid is at the same temperature as that of the lower channel wall (Figure 3a).

This, in turn, leads to higher thermal gradient near the upper wall of the channel, as shown in Figure 3b. From Figure 4a and b, we notice that the concentration surface is somewhat similar to that of thermal distribution. But, contrarily, the gradient near the upper channel wall is not as much dominating.

For presenting an understanding of the influence of the relevant parameters on different aspects of the problem, we study how, at any arbitrary time level (we have considered t=2 in our work), these parameters affect the different profiles. A rise in the value of the rheological parameter  $\beta$  physically means that the fluid acquires Newtonian character, thus meaning a lowering of the

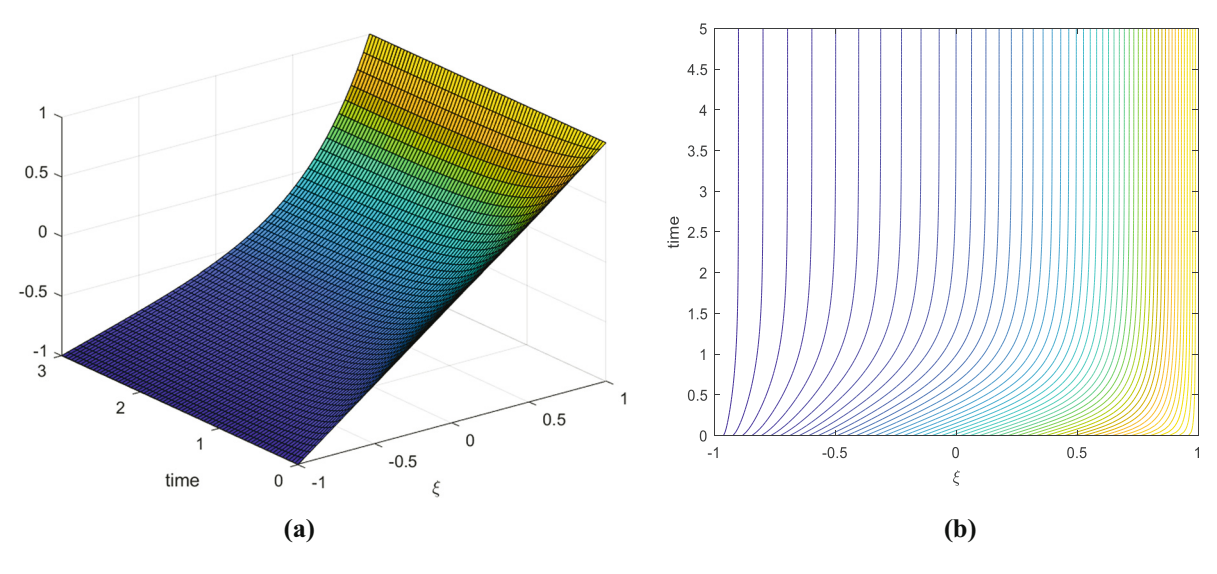
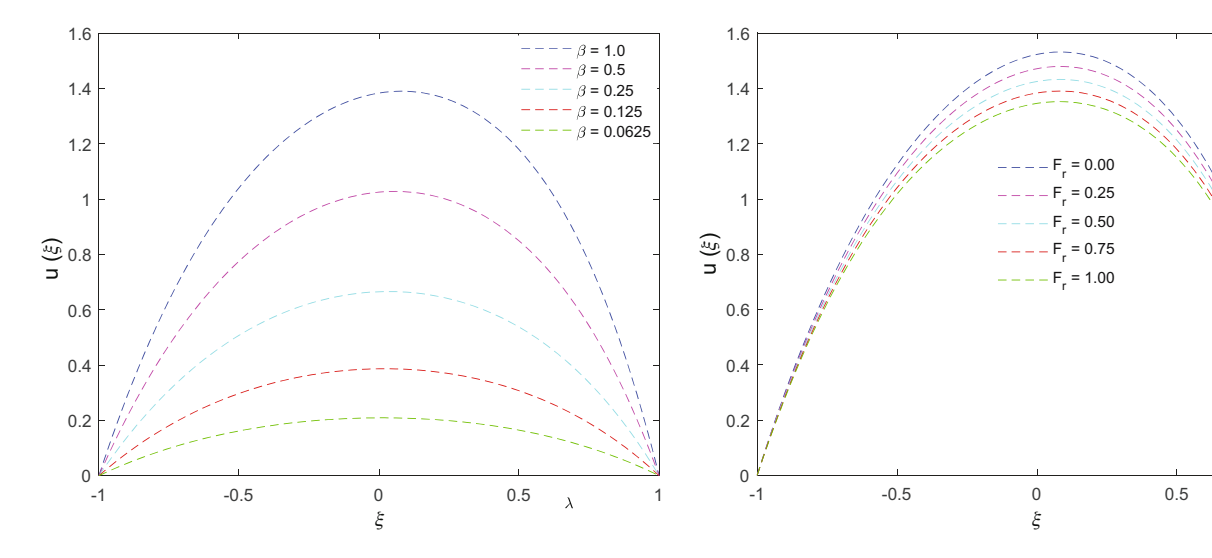


Figure 4: (a) Variation in the concentration field, with time and (b) contours of concentration field across the channel.



**Figure 5:** Variation in the velocity profile (at t = 2) for different values of the Casson parameter.

**Figure 7:** Variation in the velocity profile (at t = 2) for different values of the Forchheimer parameter.

viscosity which in turn translates into the flow acceleration under the same magnitude of the driving force (external pressure gradient), as the parameter  $\beta$  increases. This phenomenon may be observed from Figure 5.

It may be noted from Figure 6 that the Darcy parameter  $\lambda$  facilitates the flow velocity. The reason behind this is the weakening of the Darcian force (which acts as a frictional or resistive force) with increasing  $\lambda$ , appearing in the mathematical model, which turns into a greater impact of the pressure gradient on the flow. The term  $F_{\rm r}u^2$  arises in the governing equations due to the application of the Forchheimer law for modeling the porous media in the present geometry. A stronger role of this

term would translate into an increased resistance to the flow, which ultimately slows down the flow across the channel (Figure 7). In order to interpret the role of the Reynolds number (Re) for the flow across the physical domain, we refer to Figure 8 which clearly indicates an addition in the flow velocity. We notice a tilt in the velocity profiles toward the upper wall. An increase in the Reynolds number translates into a rise in the suction velocity, subject to the condition that the fluid properties remain invariant. This increased suction is responsible for the tilt in the velocity profile.

A closer look at Figure 9 shows that, once the flow starts, there is a smaller region near the upper wall where

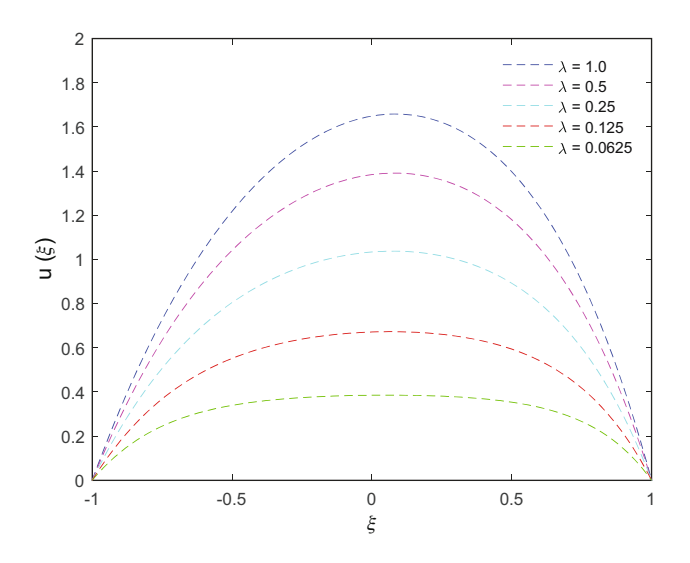


**Figure 6:** Variation in the velocity profile (at t = 2) for different values of the Darcy parameter.

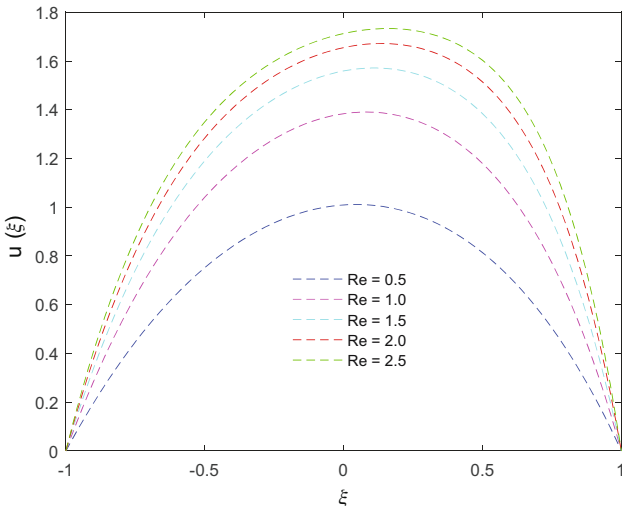


**Figure 8:** Variation in the velocity profile (at t = 2) for different values of the Reynolds number.

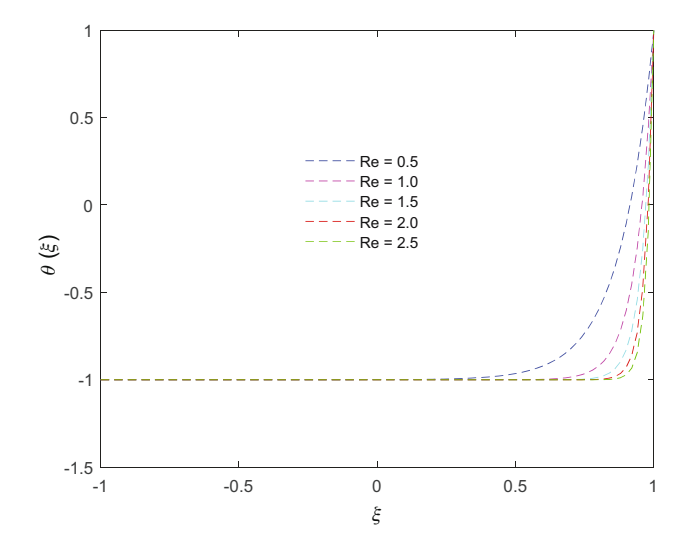


**Figure 9:** Variation in the temperature distribution (at t = 2) for different values of the Reynolds number.

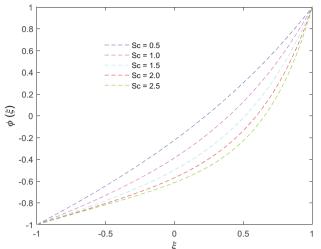


**Figure 11:** Variation in the concentration distribution (at t = 2) for different values of the Schmidt number.

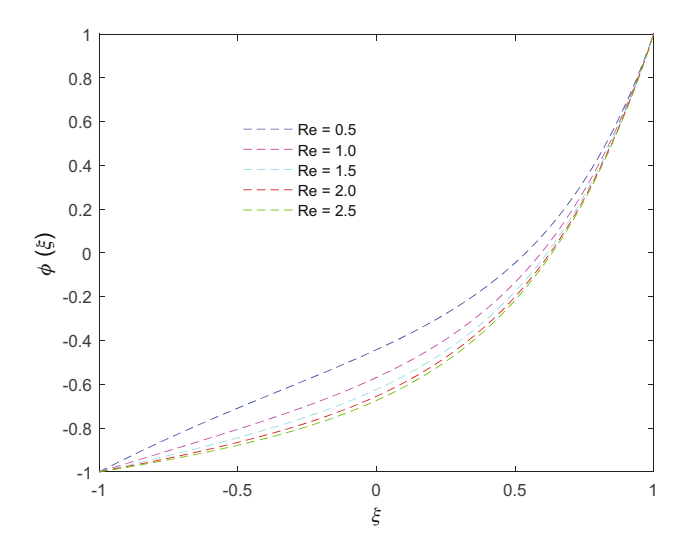


**Figure 10:** Variation in the concentration distribution (at t = 2) for different values of the Reynolds number.

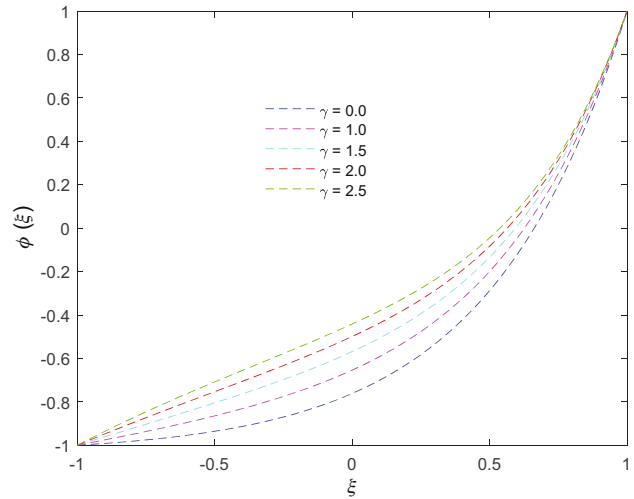


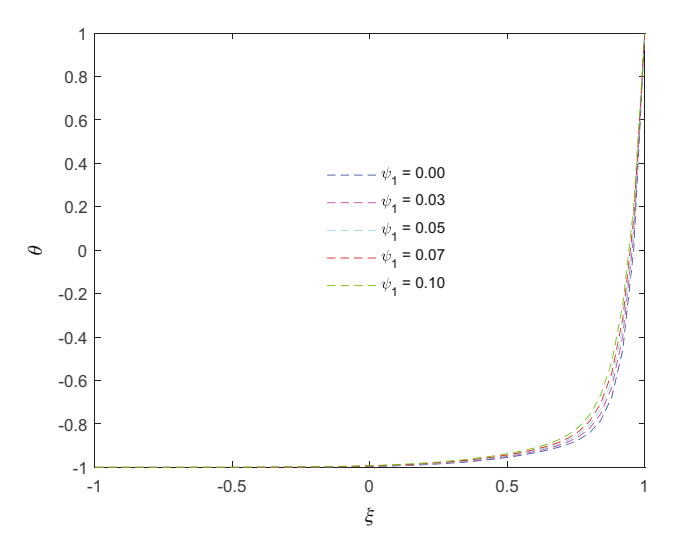
**Figure 12:** Variation in the concentration distribution (at t = 2) for different values of the chemical reaction parameter.

the temperature distribution exhibits higher gradient, thus eliminating the initial linear thermal distribution across the channel. Figures 10 and 11 show a notable decrease in the concentration profiles, with both the parameters Re and Sc. On the contrary, the chemical reaction parameter has raised the profiles, as may be seen from Figure 12. With the concentration of both type of nanoparticles, a rise in the thermal distribution is seen (Figures 13 and 14), as expected.

The consequences of Figures 15 and 16 evidently portray that the effect of both parameters (Hartmann number as well as Eckert number) is to upsurge the temperature in the flow regime. It is to point out that the pressure gradient

(which is the only deriving force for the flow, in the present problem) possesses both the steady and oscillatory components (denoted by  $p_{\rm s}$  and  $p_{\rm 0}$ , respectively). It is obvious that the steady component contributes to the flow velocity whereas the role of the oscillatory component is dependent on the nature of the term  $\cos(\omega t)$ . When the term is negative, it reduces the external force acting on the system, and thus slows down the flow. However, in the other case, it simply accelerates the flow. No figure has been drawn for the purpose, as the phenomenon may be well understood from the physics of the problem.

It has come to notice that shear stress got reduced at both channel walls with the positive change in the values



0.8

0.6

0.4

0.2

-0.2

-0.4

-0.6

-0.8

-1

-1

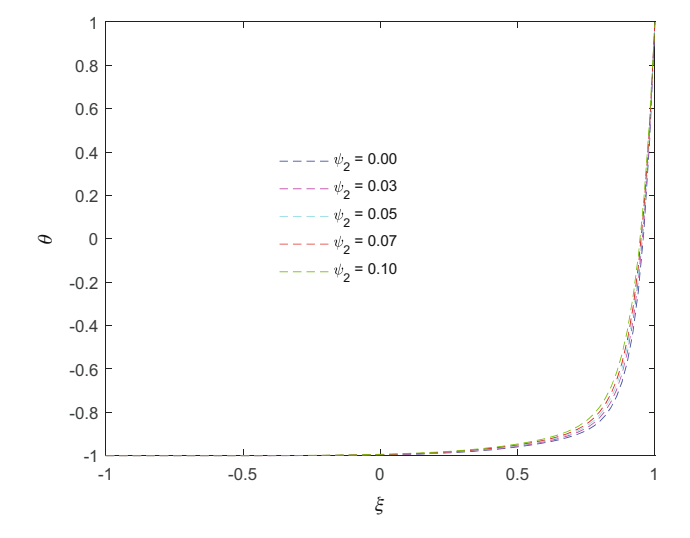
-0.5

0.5

0.5

**Figure 13:** Variation in the temperature distribution (at t = 2) for different values of the Cu nanoparticles volume concentration.

**Figure 15:** Variation in the temperature distribution (at *t* = 2) for different values of the Hartmann number.



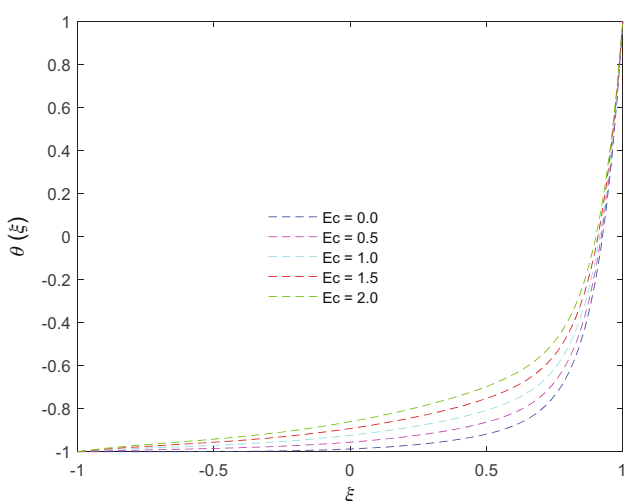


**Figure 14:** Variation in the temperature distribution (at t = 2) for different values of the Fe<sub>3</sub>O<sub>4</sub> nanoparticles volume concentration.

**Figure 16:** Variation in the temperature distribution (at t = 2) for different values of the Eckert number.

**Table 3:** Change in shear stress and heat transfer rate with M and  $\phi_1$  at upper wall

М	λ = 1	λ = 2	λ = 3	λ = 4	$\phi_1$	$\phi_2 = 0$	$\phi_2 = 0.05$	$\phi_2 = 0.10$	$\phi_2 = 0.20$
	Shear stress at the upper wall					Heat transfer rate at the upper wall			
0	1.2942	1.4326	1.4877	1.5172	0.0	4.1304	4.1813	4.2424	4.4028
1	1.1503	1.2496	1.2880	1.3084	0.05	4.1984	4.2636	4.3408	4.5388
2	1.0422	1.1173	1.1457	1.1606	0.10	4.2833	4.3646	4.4594	4.6973
3	0.9576	1.0167	1.0387	1.0501	0.15	4.3891	4.4881	4.6018	4.8811
4	0.8893	0.9372	0.9548	0.9639	0.20	4.5206	4.6385	4.7722	5.0936

М	λ = 1	λ = 2	λ = 3	λ = 4	$\phi_1$	$\phi_2 = 0$	$\phi_2 = 0.05$	$\phi_2 = 0.10$	$\phi_2 = 0.20$
	Shear stress at the lower wall						Heat transfer ra	ate at the lower	wall
0	0.9251	1.0038	1.0349	1.0515	0.0	0.0800	0.1194	0.1720	0.3267
1	0.8418	0.8994	0.9215	0.9331	0.05	0.1317	0.1883	0.2607	0.4611
2	0.7781	0.8225	0.8391	0.8479	0.10	0.2054	0.2820	0.3762	0.6238
3	0.7272	0.7628	0.7760	0.7828	0.15	0.3060	0.4045	0.5215	0.8163
4	0.6853	0.7147	0.7255	0.7310	0.20	0.4385	0.5598	0.6999	1.0406

**Table 4:** Change in shear stress and heat transfer rate with M and  $\phi_1$  at lower wall

of magnetic field parameter. On the other side, heat transfer rate significantly enhances with the effect of solid nanoparticles volume fraction  $\phi_1$  (Tables 3 and 4).

5 Conclusion

In the present work, the features of fluid flow subject to Dracy Forchheimer medium under the combined effects of MDH and pressure gradients are investigated. The interaction of various preeminent parameters with the rheological properties is noticed and prescribed for velocity and temperature distributions through the boundary layer regions. An explicit RK method is utilized for the numerical simulations. Significant outcomes of the current study are enlisted as follows:

- The maximum flow velocity during the first cycle is relatively lower, due to the pressure gradient, as compared to the case when the flow acquires certain momentum after some time.
- The greater impact of the pressure gradient on the flow is noticed, and the Darcy parameter  $\lambda$  facilitates the flow velocity.
- An increased resistance in the flow is due to the Darcian drag force which ultimately slows down the flow across the channel.
- It is obvious, from the consequences, that the steady component of the pressure gradient contributes to the flow velocity whereas the role of the oscillatory component is dependent on the nature of the term  $\cos(\omega t)$ .
- An increase in the Reynolds number translates into a rise in the suction velocity which is responsible for the tilt in the velocity profile.
- A significant decrease in the concentration profiles is noticed for both the parameters Re and Sc.

**Funding information:** This work is supported by the Natural Science Foundation of Xinjiang, China (2021D01C003).

**Author contributions:** All authors have accepted responsibility for the entire content of this manuscript and approved its submission.

**Conflict of interest:** The authors state no conflict of interest.

#### References

- [1] Thomas KN, Gibbons TD, Campbell HA, Cotter JD, Aan Rij AM. Pulsatile flow in venous perforators of the lower limb. Am J Physiol, Reg Integr Comp Physiol. 2022;323(1):R59–67. doi: 10.1152/ajpregu. 00013.2022.
- [2] Ryu C, Park J, Jung SI, Jang IR, Kim HJ. Measurement of pulsating flow using a self-attachable flexible strain sensor based on adhesive PDMS and CNT. Chemosensors. 2022;10:187. doi: 10.3390/ chemosensors10050187.
- [3] Siddique JI, Ahmed A, Aziz A, Khalique CM. A Review of mixture theory for deformable porous media and applications. Appl Sci. 2017;7:917. doi: 10.3390/app7090917.
- [4] Shamshuddin MD, Mishra SR, Anwar Beg O, Kadir A. Adomian decomposition method simulation of von Kármán swrling bioconvection nanofluid flow. J Cent South Univ. 2019;26:2797–813.
- [5] Ali K, Ahmad S, Tayebi T, Ashraf M, Jamshed W, Abd-Elmonem A, et al. Thermal attributes of hybrid (MWCNT-NiZnFe<sub>2</sub>O<sub>4</sub>) nanofluid flow having motile microbes and activation energy: A computational approach. Case Stud Therm Eng. 2023;47:103088. doi: 10.1016/j.csite.2023.103088.
- [6] Ahmad G, Abd-Elkader, Allam DF, Tag El Din ESM. Islanding detection method for DFIG wind turbines using artificial neural networks. Int J Electr Power Energy Syst. 2014;62:335–43. doi: 10.1016/j.ijepes.2014.04.052.
- [7] Afzal K, Aziz A. Transport and heat transfer of time dependent MHD slip flow of nanofluids in solar collectors with variable thermal conductivity and thermal radiation. Res Phys. 2016;6:746–53. doi: 10.1016/j.rinp.2016.09.017.
- [8] Cheffar L, Benslimane A, Sadaoui D, Benchabane A, Bekkour K. Pulsatile flow of thixotropic blood in artery under external body acceleration. Comput Meth Biomech Biomed Eng. 2023;26:927–40. doi: 10.1080/10255842.2022.2098677.
- [9] Praljak N, Ryan SD, Resnick A. Pulsatile flow through idealized renal tubules: Fluid-structure interaction and dynamic pathologies. Math Biosci Eng. 2020;17(2):1787–807. doi: 10.3934/mbe.2020094.

- [10] Mittal R, Simmons S, Najjar F. Numerical study of pulsatile flow in a constricted channel. J Fluid Mech. 2003;485:337–78. doi: 10.1017/ S002211200300449X.
- [11] Painter PR, Edén P, Bengtsson HU. Pulsatile blood flow, shear force, energy dissipation and Murray's Law. Theor Biol Med Model. 2006;3:31. doi: 10.1186/1742-4682-3-31.
- [12] Amos E, Ogulu A. Modeling pulsatile blood flow within a homogeneous porous bed in the presence of a uniform magnetic field. Int Commun Heat Mass Transf. 2002;34:989–95.
- [13] Bandyopadhyay S, Layek GC. Study of magnetohydrodynamic pulsatile flow in a constricted channel. Commun Nonlinear Sci Numer Simul. 2012;17(6):2434–46.
- [14] Eldesoky IM. Effect of relaxation time on MHD pulsatile flow of blood through porous medium in an artery under the effect of periodic body acceleration. J Biol Syst. 2013;21(2):1350011.
- [15] Abbas Z, Shabbir MS, Ali N. Numerical study of magnetohydrodynamic pulsatile flow of Sutterby fluid through an inclined overlapping arterial stenosis in the presence of periodic body acceleration. Res Phys. 2018;9:753–62.
- [16] Ali K, Ahmad S, Ashraf M. Numerical simulation of MHD pulsatile flow of a biofluid in a channel. AIP Adv. 2015;5:087130. doi: 10.1063/ 1.4928574.
- [17] Zeeshan A, Awais M, Alzahrani F, Shehzad N. Energy analysis of non-Newtonian nanofluid flow over parabola of revolution on the horizontal surface with catalytic chemical reaction. Heat Transf. 2021;50(6):6189–6209.
- [18] Ahmad S, Ali K, Ashraf M, Khalifa HAE, ElSeabee FAZ, Tag El Din ESM. Analysis of pure nanofluid (GO/engine oil) and hybrid nanofluid (GO–Fe<sub>3</sub>O<sub>4</sub>/engine oil): Novel thermal and magnetic features. Nanotechnol Rev. 2022;11:2903–15.
- [19] Pattnaik PK, Mishra SR, Anwar Bég O, Khan UF, Umavathi JC. Axisymmetric radiative titanium dioxide magnetic nanofluid flow on a stretching cylinder with homogeneous/heterogeneous reactions in Darcy-Forchheimer porous media: Intelligent nanocoating simulation. Mater Sci Eng B. 2022;277:115589.
- [20] Salahuddin T, Awais M, Xia F. Variable thermo-physical characteristics of Carreau fluid flow by means of stretchable paraboloid surface with activation energy and heat generation. Case Stud Therm Eng. 2021;25:100971. doi: 10.1016/j.csite.2021.100971.
- [21] Salahuddin T, Mahmood Z, Khan M, Awais M. A permeable squeezed flow analysis of Maxwell fluid near a sensor surface with radiation and chemical reaction. Chem Phys. 2022:562:111627.
- [22] Salahuddin T, Ali Z, Awais M, Khan M, Altanji M. A flow behavior of Sutterby nanofluid near the catalytic parabolic surface. Int Commun Heat Mass Transf. 2022;131:105821. doi: 10.1016/j. icheatmasstransfer.2021.105821.
- [23] Karmakar P, Ali A, Das S. Circulation of blood loaded with trihybrid nanoparticles via electro-osmotic pumping in an eccentric endo-

- scopic arterial canal. Int Commun Heat Mass Transf. 2023:141:106593.
- [24] Rajamani S, Reddy AS. Effects of Joule heating, thermal radiation on MHD pulsating flow of a couple stress hybrid nanofluid in a permeable channel. Nonlinear Analysis: Model Control. 2022;27(4):684–99. doi: 10.15388/namc.2022.27.26741.
- [25] Govindarajulu K, Reddy AS. Magnetohydrodynamic pulsatile flow of third grade hybrid nanofluid in a porous channel with Ohmic heating and thermal radiation effects. Phys Fluids. 2022;34:013105. doi: 10.1063/5.0074894.
- [26] Selimefendigil F. Pulsating hybrid nanofluids double slot jets impingement onto an isothermal wall. 2018;49(2):173–88. doi: 10.1615/HeatTransRes.2017015650.
- [27] Manchi R, Ponalagusamy R. Pulsatile flow of EMHD micropolar hybrid nanofluid in a porous bifurcated artery with an overlapping stenosis in the presence of body acceleration and Joule heating.

  Braz J Phys. 2022;52:52.
- [28] Bukhari Z, Ali A, Abbas Z, Farooq H. The pulsatile flow of thermally developed non-Newtonian Casson fluid in a channel with constricted walls. AIP Adv. 2021;11:025324. doi: 10.1063/5.0036738.
- [29] Jamshed W, Aziz A. A comparative entropy based analysis of Cu and Fe<sub>3</sub>O<sub>4</sub>/methanol Powell-Eyring nanofluid in solar thermal collectors subjected to thermal radiation, variable thermal conductivity and impact of different nanoparticles shape. Results Phys. 2018;9:195–205. doi: 10.1016/j.rinp.2018.01.063.
- [30] Pattnaik PK, Pattnaik JR, Mishra SR, Nisar KS. Variation of the shape of  $\text{Fe}_3\text{O}_4$ -nanoparticles on the heat transfer phenomenon with the inclusion of thermal radiation. J Therm Anal Calorim. 2022;147:2537–48. doi: 10.1007/s10973-021-10605-9.
- [31] Karmakar P, Das S. Electro-blood circulation fusing gold and alumina nanoparticles in a diverging fatty artery. BioNanoSci. 2023:13:541–63
- [32] Ali A, Barman A, Das S. EDL aspect in cilia-regulated bloodstream infused with hybridized nanoparticles via a microtube under a strong field of magnetic attraction. Therm Sci Eng Prog. 2022;36:101510. doi: 10.1016/j.tsep.2022.101510.
- [33] Ali K, Ahmad S, Ahmad S, Jamshed W, Hussain SM, Tag El Din ESM. Molecular interaction and magnetic dipole effects on fully developed nanofluid flowing via a vertical duct applying finite volume methodology. Symmetry. 2022;14:2007. doi: 10.3390/sym14102007.
- [34] Taha A, Aziz A, Khalique CM. Exact solutions for stokes' flow of a non-Newtonian nanofluid model: A Lie similarity approach. Z für Naturforschung A. 2016;71(7):621–30. doi: 10.1515/zna-2016-0031.
- [35] Nakamura M, Sawada T. Numerical study on the flow of a non-Newtonian fluid through an axisymmetric stenosis. J Biomech Eng. 1988 May;110(2):137–43. doi: 10.1115/1.3108418PMID: 3379935.
- [36] Ashraf M, Ali K, Ashraf MM. Numerical simulation of micropolar flow in a channel under oscillatory pressure gradient. Iran J Chem Chem Eng. 2020;39:263–72.